Journal of Crystal Growth 451 (2016) 72–78

Contents lists available at ScienceDirect

Journal of Crystal Growth

journal homepage: www.elsevier.com/locate/jcrysgro

Synthesis of nanoporous carbohydrate metal-organic framework and encapsulation of acetaldehyde

Saleh Al-Ghamdi [a], Ajay Kathuria [b,*], Mohamad Abiad [c,d], Rafael Auras [d,*]

[a] Department of Agricultural Engineering, College of Food and Agricultural Sciences, King Saud University, P.O. Box 2460, Riyadh 11451, Saudi Arabia
[b] Industrial Technology and Packaging, California Polytechnic State University, San Luis Obispo, CA 93407, USA
[c] Department of Nutrition and Food Sciences, American University of Beirut, P.O. Box 11-0236, Riad El Solh, Beirut 1107-2020, Lebanon
[d] School of Packaging, Michigan State University, East Lansing, MI 48824, USA

ARTICLE INFO

Article history:
Received 6 April 2016
Received in revised form
29 June 2016
Accepted 5 July 2016
Available online 6 July 2016

Keywords:
A1. Biomaterials
B1. Nanomaterials
A1. Adsorption
B1. Organic compounds
A2. Growth from solutions
A1. Diffusion

ABSTRACT

Gamma cyclodextrin (γ-CD) metal organic frameworks (CDMOFs) were synthesized by coordinating γ-CDs with potassium hydroxide (KOH), referred hereafter as CDMOF-a, and potassium benzoate ($C_7H_5KO_2$), denoted as CDMOF-b. The obtained CDMOF structures were characterized using nitrogen sorption isotherm, thermo-gravimetric analysis (TGA), X-ray diffraction (XRD), and scanning electron microscopy (SEM). High surface areas were achieved by the γ-CD based MOF structures where the Langmuir specific surface areas (SSA) of CDMOF-a and CDMOF-b were determined as 1376 $m^2 g^{-1}$ and 607 $m^2 g^{-1}$; respectively. The dehydrated CDMOF structures demonstrated good thermal stability up to 250 °C as observed by the TGA studies. XRD results for CDMOF-a and CDMOF-b reveal a body centered-cubic (BCC) and trigonal crystal system; respectively. Due to its accessible porous structure and high surface area, acetaldehyde was successfully encapsulated in CDMOF-b. During the release kinetic studies, we observed peak release of 53 μg of acetaldehyde per g of CDMOF-b, which was 100 times greater than previously reported encapsulation in β-CD. However, aldol condensation reaction occurred during encapsulation of acetaldehyde into CDMOF-a. This research work demonstrates the potential to encapsulate volatile organic compounds in CDMOF-b, and their associated release for applications including food, pharmaceuticals and packaging.

1. Introduction

Cyclodextrins (CDs) are naturally synthesized from starch using glycosyltransferase enzymes. These cyclic structures exist in various forms including alpha (α), beta (β), gamma (γ) and delta (δ) form [1]. The difference among these forms is attributed to the numbers of 1,4-linked glucopyranose units which are attached in a cyclic arrangement. The α, β, γ, and δ forms have 6, 7, 8, and 9 glucopyranose units; respectively. As a result, the molecular weight of CDs varies from 972 to 1459 g mol^{-1} while their cavity diameter ranges between 0.47 and 0.83 nm; respectively [2]. One of the most remarkable properties of CDs is their ability to form inclusion complexes (ICs) with volatile organic compounds due to their hydrophilic exterior and hydrophobic interior. In such complexes, the volatile compounds are entrapped inside the hydrophobic CD pores due to secondary interactions. Such ICs have been widely explored because of their potential applications in pharmaceutical [3], chemical [4], food and packaging industries [5–7].

Several researchers have studied CD based ICs. The ability of CDs to host a guest molecule depends on various factors such as the size of the guest molecule, the pore size of the CDs, chemical interactions between functional groups of the guest molecule and hydrophobic pore interior. Veiga et al. [8] prepared tolbutamide urea (TBM) β-CD complexes using kneading, freeze-drying and co-precipitation. The study concluded increased solubility, dissolution and oral bioavailability of TBM due to the ICs. Almenar et al. [9] studied post-harvest fungal decay inhibition efficacy of acetaldehyde released from α, β or γ-CD acetaldehyde ICs. Effective fungal decay was observed when β-CD acetaldehyde IC was employed during the marketable period. In another study, Almenar et al. [10] also prepared hexanal and β-CD ICs in distilled water with different concentrations. The authors encapsulated a maximum of 1.40 ppb hexanal in β-CD, and reported that the released hexanal was effective against the growth of fungi. Although β-CD allows the encapsulation of organic compounds through ICs, the total amount that can be absorbed and later released is still relatively low.

Metal-organic frameworks (MOFs) are a new class of

* Corresponding authors.
E-mail addresses: akathuri@calpoly.edu (A. Kathuria), aurasraf@msu.edu (R. Auras).

http://dx.doi.org/10.1016/j.jcrysgro.2016.07.004
0022-0248/

microporous coordination polymers, which consists of metal ions and organic linkers [11]. MOFs are well known for their high surface area, gas sorption, gas separation, selectivity and chemical sensing [12–15]. The structural properties of MOFs are unique among other materials including organic, inorganic and hybrid porous structures such as zeolite and activated carbon. These distinctive properties can be accredited to the high porosity of MOFs and their reticulate symmetrical structures, which allow them to host guest molecules like H_2, CO_2, N_2 and CH_4 [16–18].

Recently, cyclic macromolecules such as CDs [19–22], crown ethers [23], pillararenes [24] and cucurbiturils [25] with inherently large cavities have been utilized as organic struts for synthesizing MOFs. Such structures offer two porosity levels, the first one exists naturally in these cyclic macromolecules, and the second is created as the result of the chemical coordination between these struts and the metal ions. Gamma CD, a cyclic macromolecule, has been recently coordinated with earth metal ions (*e.g.,* K^+, Rb^+, Na^+, and Cs^+) to obtain cyclodextrin based metal organic frameworks (CDMOFs) [19]. Gassensmith et al. [20] utilized γ-CD and Rb^+ ions based MOF structure, also known as CDMOF-2, for sensing and quantification of CO_2 using electrochemical impedance spectroscopy. They credited reversible chemisorption of CO_2 to electrochemical sensing of CDMOF-2. Yoon et al. fabricated [21] metal/MOF/metal hetero-structures based memristors using single crystals of CDMOF-2 for storage of electrical information. The ability of these hetero-structures to work as resistive random-access memory (RRAM) was ascribed to the porous structure of MOFs, which allows transportation of ions when infused with electrolytes. The release of drug encapsulation in the γ-CD and K^+ ion MOF structure, generally known as CDMOF-1, has been studied for drug carrier applications using Monte Carlo simulations [22]. In their study, researchers observed strong interactions between the metal centers of the MOF and the carbonyl group present in the analgesic drug, ibuprofen [22].

In this study, we synthesized two different γ-CD-K^+ ions based MOFs using potassium hydroxide and potassium benzoate as sources of K^+ ion, referred hereafter as CDMOF-a and CDMOF-b; respectively. Gamma-CDs were chosen as linkers due to their bio-based nature as well as their unique ability to form ICs. These CDMOFs were synthesized because of the non-toxic nature of alkali metals, presence of polar groups, open metal sites and the ability of various CDs to form ICs [26–28]. The main objectives of this study were: a) to synthesize CDMOF-a and CDMOF-b; b) to determine the physical and thermal characteristics of CDMOF-a and CDMOF-b crystals; and c) to run a proof-of-concept of the ability of CDMOFs to encapsulate and release a selected organic compound, acetaldehyde, which is known for its anti-fungal activity [9]. To the best of the authors' knowledge, no study has focused on encapsulation and release kinetics of acetaldehyde in CDMOFs.

2. Methodology

2.1. Materials

Gamma CD (purity $>99\%$, food grade) was donated by Wacker Chemical Corporation (Adrian, MI, USA). Potassium hydroxide (KOH) pellets (ACS reagent, purity $\geq 85\%$), and potassium benzoate ($C_7H_5KO_2$) were purchased from Columbus Chemical Industries, Inc. (Phoenix, AZ, USA). Anhydrous methanol (purity $>99.8\%$) and acetaldehyde (purity $\geq 99\%$, FCC) were purchased from Sigma-Aldrich Corp. (Saint Louis, MO, USA). Distilled and deionized water was purchased from Avantor Performance Materials (Center Valley, PA, USA). All materials were used as received unless otherwise indicated.

2.2. Synthesis and activation of CDMOF

The CDMOFs were synthesized as per Smaldone et al. [26]. One mmol (1.30 g) of γ-cyclodextrin and 8 mmol (0.45 g) of KOH were dissolved in 20 mL of deionized water and labeled in this work as CDMOF-a. On the other hand, 1.6 mmol (0.256 g) of $C_7H_5KO_2$ and 0.2 mmol (0.26 g) of γ-CD were diluted in 5 mL of deionized water to synthesize CDMOF-b. The solutions were stirred continuously for 6 h at 500 rpm followed by slow vapor diffusion of methanol over a period of 3 to 7 d. After the CDMOF crystals were produced in the solution with an average yield of 1.25 g for the CD and KOH, and 0.30 g for the CD and $C_7H_5KO_2$, the crystals were washed with methanol to remove unreacted potassium ions and then filtered (samples were labeled as as-synthesized). After synthesis, the CDMOFs were activated in a vacuum oven at 23 °C for 10 h at 4 kPa (30 mmHg). Then, the temperature was increased to 45 °C and maintained for an additional 12 h under the same vacuum pressure 4 kPa (samples were labeled as activated).

2.3. Surface area and pore size

The gas sorption experiments were conducted using an iQMicropore-XR (Quantachrome Instruments, Boynton Beach, FL, USA). The surface area, pore sizes and diameters of the CDMOFs were calculated using the Brunauer-Emmett-Teller (BET) and Langmuir methods. Samples weighing 0.05 g of each synthesized CDMOF-a and CDMOF-b crystals were dehydrated for 10 h of vacuum pressure at 0.133 kPa (1 Torr) at 25±0.1 °C followed by heating at 45 °C for 12 h under the same pressure. The specimens were then transferred to the sorption station where the N_2 adsorption took place at 77.3 K and N_2 gas sorption at a relative pressure varying from 10^{-5} to 0.99 [29].

2.4. Thermogravimetric analysis (TGA)

Thermal stability of CDMOF-a and CDMOF-b crystals were evaluated using a TGA model 2950, from TA Instruments (New Castle, DE, USA). A sample weight of 5 mg of activated CDMOF-a and CDMOF-b were utilized to perform the studies. Samples were heated from 25 to 450 °C at a rate of 10 °C min^{-1}. Data were collected and analyzed using the Universal Analysis software version 2000 from TA Instruments.

2.5. X-ray diffraction (XRD)

The CDMOF-a and CDMOF-b activated crystals were examined using a Bruker D8 advance X-ray diffractometer (Bruker AXS GmbH, Karlsruhe, Germany) using Cu Kα ($\lambda=0.154$ nm) radiations at 40 kV, 40 mA. The samples were studied using 1.2 mm primary beam slit, and 2.0 mm detector slit over 3 to 40° 2 theta angles with increments at 0.02° per min.

2.6. Scanning electron microscopy (SEM)

To study the topography, activated CDMOF-a and CDMOF-b crystals were sputter coated with approx. 8 nm thick platinum coating. The coated specimens were examined using a JEOL JSM 6410 LV (JEOL Ltd., Tokyo, Japan) SEM, equipped with a tungsten filament, at 10 kV accelerating voltage.

2.7. Encapsulation and release method

Acetaldehyde encapsulation was carried out after activating the CDMOF-a and CDMOF-b. First, 1 g of activated CDMOF-a or CDMOF-b was placed in a small aluminum pan that was placed in a 2 L glass jar. Acetaldehyde (1 mL), previously stored in a

conventional refrigerator at 5 °C, was injected in the jar by airtight micro-syringe at the same temperature and placed into a PTC-1 Temperature Cabinet at 25 ± 0.1 °C with a controller device from Sable System International, NA, USA. The glass jar was sealed with a metal screw cap for 24 h in the chamber to insure the acetaldehyde penetration in the CDMOFs voids (*samples were labeled as encapsulated*).

The release amount of acetaldehyde from the encapsulated CDMOFs was determined by transferring the encapsulated CDMOFs to a new 2 L glass jar. The acetaldehyde concentration in the headspace was measured at 25 ± 0.1 °C. A gas chromatographer (GC), from Hewlett Packard GC 6890, CA, USA, with a flame ionization detector (FID) and a HP-5 column dimension 30 m × 0.32 mm × 0.25 μm, was used to determine the headspace concentration of acetaldehyde release in the jar. An airtight gas micro-syringe was used to extract 25 μL from the jar headspace through a rubber septum placed in the metal screw lid and injected into the GC. Samples (25 μL) from the headspace were injected to the GC at 1, 2, 3, 4, 5, 6, and 24 h after the encapsulated CDMOFs were introduced in the 2 L jar. The GC setting conditions were as follows; oven temperature initially 80 °C for 2 min, and increased to 200 °C at 10 °C min^{-1}. The detector and the inlet temperatures were at 240 °C. A calibration curve between 50 to 500 μL/L of acetaldehyde concentration was constructed at 25 ± 0.1 °C with an adjusted R-square =0.990. Samples were tested in triplicate.

2.8. Color measurements

Encapsulated CDMOF-a and CDMOF-b specimens were examined using a Mold U-4100 HunterLab LabScan XE (Reston, VA, USA) colorimeter for color changes after 24 h of activation and after encapsulation. L^* Lightness, a^* from red positive to green negative, b^* from yellow positive to blue negative were obtained. ΔE total color change was calculated using the equation $\Delta E=[(\Delta L^*)^2 + (\Delta a^*)^2 + (\Delta b^*)^2]^{1/2}$.

2.9. Data analysis

The entire data were analyzed using Tukey's HSD (Honestly Significant Differences) for the means comparisons with $\alpha=0.05$ at 95% confidence interval using SAS 9.4 Software (SAS Institute Inc., Cary, NC, USA).

3. Results and discussion

3.1. Synthesis and activation of CDMOF

CDMOF-a and CDMOF-b were successfully produced with KOH and $C_7H_5KO_2$ respectively by using vapor diffusion crystallization process at room temperature (23 °C). Methanol, a popular solvent for crystal growth, was used because its high vapor pressure and reasonably good solubility aids the crystal growth. CDMOF-b crystals synthesized in 2–3 d whereas CDMOF-a crystal took approximately 1.3 d to crystallize from the solution, indicating the slow nucleation rate in γ-CD- $C_7H_5KO_2$ solution and CDMOF-b crystal growth as compared to CDMOF-a, which may be affected by various factors such as the basicity of the solution, source of the metal ions, synthesis methodology and reactants concentration [30,31]. Biemmi et al. [30] examined three different sources of Zn: (i) Zinc (II) Nitrate ($Zn(NO_3)_2 \cdot 6H_2O$), (ii) Zinc acetate ($Zn(CH_3COO)_2 \cdot 2H_2O$), and (iii) Zinc Oxide (ZnO), for the synthesis of MOF-5. Although, MOF-5 synthesized using all the three Zn sources mentioned above, the metal source significantly impacted both the morphology and crystal size. Smaller crystals were reported for Zinc acetate, the authors credited it to the faster nucleation due to higher basicity as compared to Zinc nitrate. Michida et al. [28] monitored the pH of the solution during the CDMOF synthesis, and reported higher yield when the crystals are grown from solution with higher basicity. We obtained 70% yield for the synthesis of CDMOF-a crystals and 50% yield for CDMOF-b crystals. The higher yield in case of CDMOF-a may be correlated to higher basicity in the CDMOF-a solution.

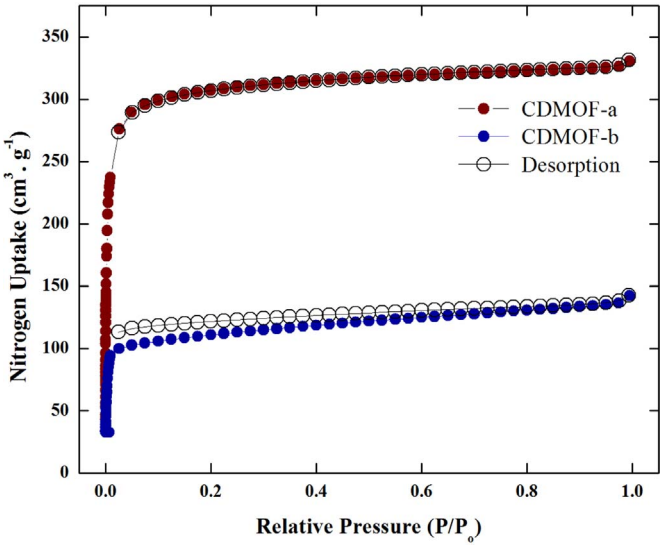

Fig. 1. N_2 sorption/desorption isotherms of CDMOF-a and CDMOF-b.

3.2. Surface area and pore size

Porous materials are meticulously tailored to achieve specific objectives. Physical characteristics such as surface area, pore size and pore volume have significant impact on the functionality, selectivity and intrinsic surface energy of these molecules. The three-dimensional coordination arrangement between organic linkers and ions significantly influences the theoretical pore volume and the surface area. The N_2 isotherms of CDMOF-a and CDMOF-b samples are represented in Fig. 1. Type-1 isotherms, also known as Langmuir isotherm, were observed for both the CDMOFs, as per International Union of Pure and Applied Chemistry (IUPAC) classification. The surface area, pore size and pore volume of CDMOF-a and CDMOF-b are summarized in Table 1. High adsorption at low partial pressure indicates microporous nature of the material and correlates with high surface energy. As observed from Table 1, CDMOF-a has more than two times the surface area of CDMOF-b. This variation between the measured surface areas may be attributed to the difference in the crystal structure of the two MOFs and presence of the benzoate counter-anions in the pores of CDMOF-b. CDMOF-a, $K_2(C_{48}H_{80}O_{40})(OH)_2$, has body centered cubic crystal structure whereas CDMOF-b,

Table 1
Surface area (SA), pore size and pore volume of CDMOF-a and CDMOF-b.

CDMOFs	BET SA ($m^2 g^{-1}$)	Langmuir SA ($m^2 g^{-1}$)	Micropore volume ($cm^3 g^{-1}$)	Total pore volume ($cm^3 g^{-1}$)	Average pore radius (nm)
CDMOF-a	1229 ± 6^a	1376 ± 18^a	0.49 ± 0.02^a	0.50 ± 0.02^a	0.79 ± 0.01^a
CDMOF-b	417 ± 110^b	607 ± 102^b	0.18 ± 0.03^b	0.22 ± 0.03^b	0.40 ± 0.40^a

Note: Values in the same column with the same superscript letters are not significantly different at $\alpha=0.05$. Micropore volumes were calculated at a radius of 2 nm, whereas total pore volumes were obtained at the relative pressure $P/P_o=0.99$.

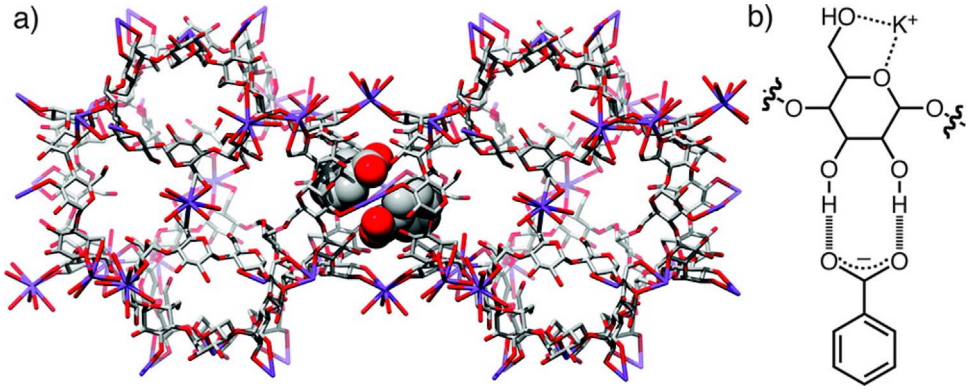

Fig. 2. (a) Location of the benzoate anion in the γ-CDMOF-b structure as stick representation of the crystal structure of CDMOF – benzoate anions are represented as space-filling mode, and (b) interactions between CD moiety and benzoate anion, reprinted with permission from Forgan et al. [32]. Copyright 2011 American Chemical Society.

$K_4(C_{96}H_{160}O_{80})(C_7H_5O_2)_2$-$(OH)_2$ has trigonal crystal structure [26,32] .

The theoretical pore density of CDMOF-a has been calculated as 0.56 g cm^{-3} [26], which is close to the measured density ~0.50 g cm^{-3}. On another note, the micro-pore volume for CDMOF-b was measured at ~0.18 cm^3 g^{-1}, which can be attributed to the crystal structure and the fact that the pores are partly occupied by the benzoate counter-anions [26,32]. This is also in line with Forgan et al. [32] who reported the presence of stabilized benzoate counter-anions in the γ-CD dimers due to formation of two hydrogen bonds between γ-CD and benzoate anions. Fig. 2a shows the location of benzoate counter-anions in the CDMOF-b structure, and Fig. 2b represents the interactions between CD moiety and benzoate anion.

3.3. Thermogravimetric analysis (TGA)

The thermograms of CDMOF-a and CDMOF-b are represented in Fig. 3. The thermogravimetric studies indicate ~8% weight loss in CDMOF-a and CDMOF-b up to 150 °C. This weight loss can primarily be associated with the loss of water molecules residing in the pores of these MOF structures. CDMOF-b is thermally more stable as compared to CDMOF-a. The sharp weight loss in CDMOF-a around 264 °C can be ascribed to the destruction of hydroxyl groups present in the γ-CD. On the other hand, in the case of CDMOF-b the first degradation peak was observed at approximately 315 °C. Further weight loss peaked around 428 °C due to the decomposition of glucopyranose units, as observed by their derivative profiles (DTGA). Relatively higher thermal stability of the hydroxyl groups in CDMOF-b can be ascribed to the secondary interaction with the benzoate counter-anions present in the structure.

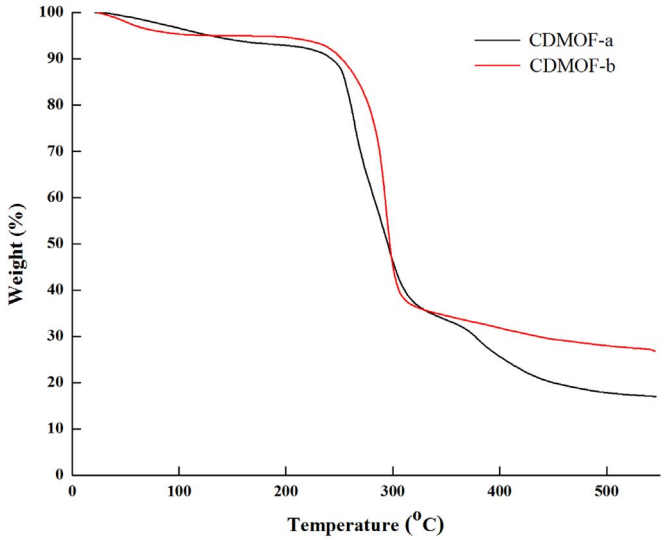

Fig. 3. Thermo-gravimetric analysis of CDMOF-a and CDMOF-b.

3.4. X-ray diffraction (XRD)

Diffraction patterns of CDMOF-a, $K_2(C_{48}H_{80}O_{40})(OH)_2$, CDMOF-b are represented in Figs. 4a and b; respectively, matching previously reported XRD patterns [26]. The details of these crystals have been previously reported [26,32] and freely accessible in the database of The Cambridge Crystallographic Data Centre under the CCDC numbers 773709 and 773711. $K_2(C_{48}H_{80}O_{40})(OH)_2$, crystals have body centered cubic crystal, and they represent space group I432 with axial lengths $a=b=c=31.006$ Å and inter-axial angles $\alpha=\beta=\gamma=90°$. The formation of cubic crystal structure has been ascribed to the eight-fold symmetry offered by γ-CD [29]. On the other hand, CDMOF-b, $K_4(C_{96}H_{160}O_{80})(C_7H_5O_2)_2(OH)_2$, has trigonal crystal system representing space group R32 with axial lengths $a=b=42.6517$ Å, $c=28.4636$ Å and inter-axial angles $\alpha=\beta=90°$, $\gamma=120°$.

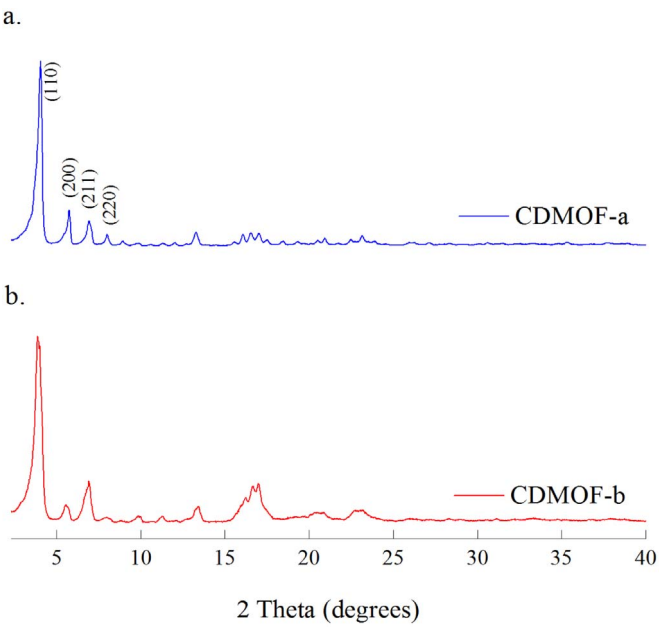

Fig. 4. X-ray diffraction of activated CDMOF-a and CDMOF-b.

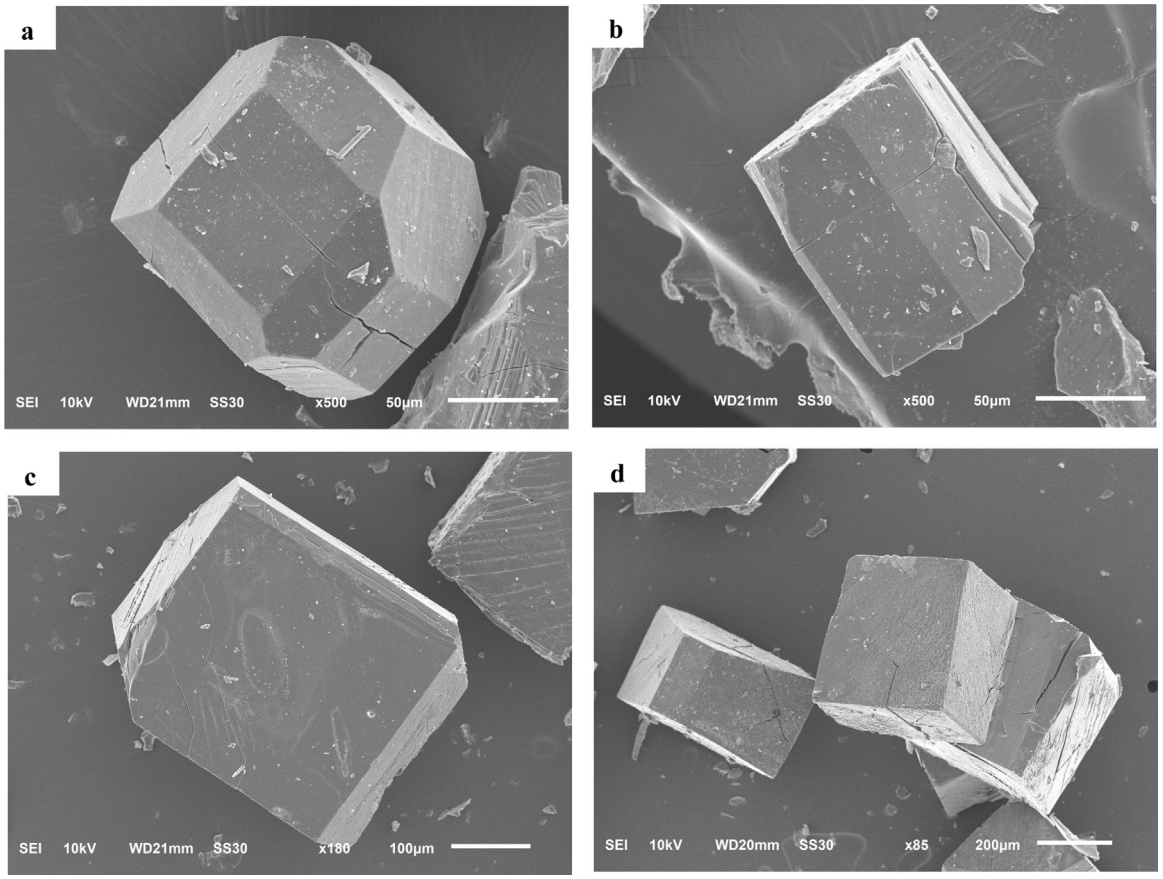

Fig. 5. (a) SEM image-I of CDMOF-a scale size 50 μm (b) SEM image-II of CDMOF-a scale size 50 μm (c) SEM image-I of CDMOF-b scale size 100 μm. (d) SEM image-II of CDMOF-b scale size 200 μm.

3.5. Scanning electron microscopy (SEM)

External shape and size of the crystal are important for employing these crystals for various industrial applications [31]. In addition, size variations can alter the physical properties of the MOF particles. Morphology, size, shape and visible appearance of a crystal are influenced by source of metal ion, solvent, impurities, nucleation, crystal growth pattern and MOF crystal synthesis parameters such as temperature and pressure [31–34]. SEM images of CDMOF-a and CDMOF-b are represented in Figs. 5a, b and c, d; respectively. CDMOF-b has twice the size of CDMOF-a. The larger size of CDMOF-b can be ascribed to lower nucleation rate and slower crystal growth [30,34], which may have been influenced by the presence of benzoate counter-anions in the solution.

3.6. Encapsulation and release of acetaldehyde

Acetaldehyde, a naturally occurring antifungal, is a chemically reactive compound. It is water-soluble and volatile in nature, which poses retention and stability challenges. Cyclodextrin inclusion complexes have been utilized for retention and delivery of controlled release of acetaldehyde [9]. Two level of pores exist in the CDMOF which can potentially host acetaldehyde **a.** pore (cavity), which exist naturally in the cyclic CD molecules with diameter ranging from 7.5–8.3 Å and **b.** pores in the MOF structure due to coordination of the CDs with the K^+ ions. Both CDMOF-a and CDMOF-b were evaluated as a proof of concept for the encapsulation of acetaldehyde. We successfully encapsulated acetaldehyde in CDMOF-b as supported by the release kinetics and TGA studies. The successful encapsulation of acetaldehyde in the γ-CDMOF-b can be ascribed to the strong quadrupole-quadrupole interactions between acetaldehyde and electron rich aromatic ring present in the benzoate counter-anion present in the MOF structure [31,35].

Wu et al. [35] studied adsorption mechanism of acetaldehyde on MOF-5 using density functional theory. They observed strong secondary interactions between aromatic rings present in the organic linkers and carbonyl group present in the acetaldehyde with adsorption energy −10 kJ/mol. They also observed that any electron withdrawing groups attached to benzene ring increases the acetaldehyde adsorption capacity of MOF-5.

The release of acetaldehyde from encapsulated CDMOF-b with time can be observed in Fig. 6. The acetaldehyde release from 1 g of CDMOF-b steadily increased and peaked to 53 μg/ after 5 h, the release quantity dropped further with time. After 24 h, the concentration of acetaldehyde in the headspace dropped to around 30 μg acetaldehyde per 1 g of CDMOF. Almenar et al. [9] observed similar trends in the acetaldehyde release kinetics study from β-CD acetaldehyde ICs. However, the peak quantity of acetaldehyde released from CDMOF-b is two order of magnitude higher than the release reported in the β-CD ICs. It can be ascribed to high acetaldehyde sorption capacity of CDMOF-b as compared to β-CD due to its high specific surface area and microporous structure of CDMOF-b. We could not find any study focused on encapsulation and release of acetaldehyde in γ-CD. Fig. 6 also shows a large release variation of acetaldehyde at higher rates, which could be attributed to preferential desorption of acetaldehyde and/or variation on efficiencies on the encapsulation method. Further assessment is required to streamline the release of acetaldehyde from CDMOF-b. However, this information provides encouraging results of a system that could create ICs with larger amount of the organic compounds.

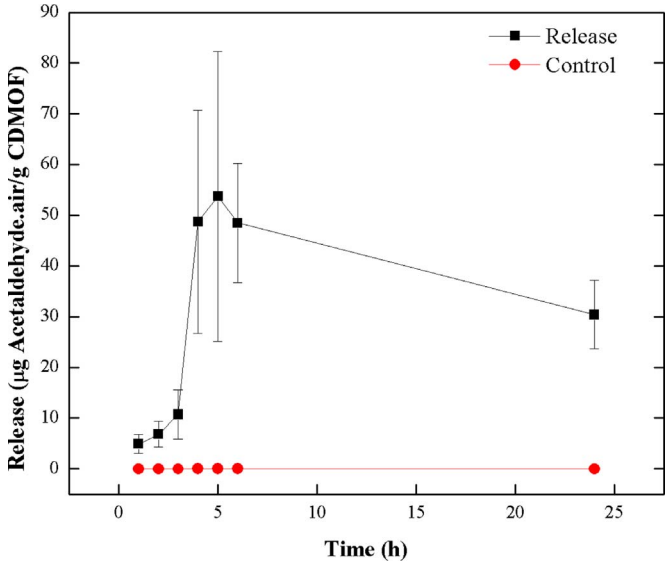

Fig. 6. Release kinetics of acetaldehyde per gram of CDMOF-b.

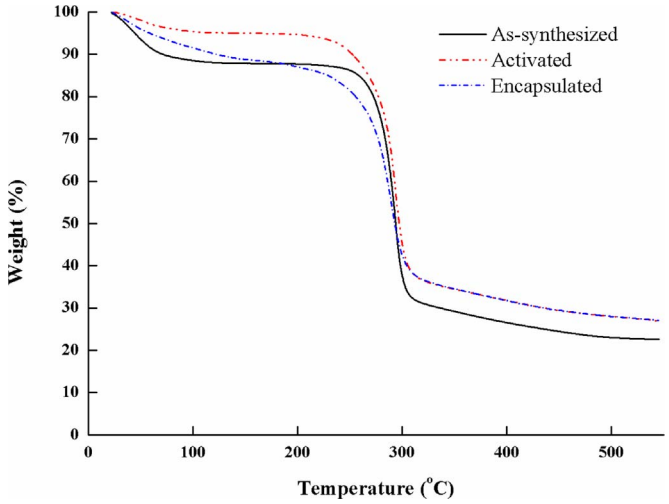

Fig. 7. Thermo-gravimetric analysis of as-synthesized, activated, and encapsulated CDMOF-b.

To estimate the total amount of acetaldehyde encapsulated in the CDMOF-b, we utilized TGA studies. Fig. 7 shows TGA thermographs of as-synthesized, activated and encapsulated CDMOF-b. All the samples demonstrated good thermal stability below 250 °C. As synthesized samples lost ~12–14% weight at 100 °C as compared to its actual weight which can be ascribed to loss of water present in the CDMOF-b pores. Activated samples lost around 4% weight, this weight could be associated with adsorption of moisture or other molecules during the handling of CDMOF-b before TGA studies. Encapsulated samples lost ~13.75 wt% at ~150 °C, which could primarily be associated with the loss of the acetaldehyde present in the CDMOF-b pores. The thermal degradation onset temperatures for as synthesized, activated and encapsulated γ-CDMOF-b were observed between 250–300 °C.

Although CDMOF-a has higher surface area than CDMOF-b, we struggled to encapsulate the acetaldehyde in CDMOF-a due to aldol self-condensation reaction, represented in Fig. 8, because of the presence of hydroxide counterions in the pore of MOF which may have released from the potassium hydroxide during the MOF synthesis. Aldol condensation was also evident as color change in the CDMOF-a crystals from white to brownish red in couple of minutes during the encapsulation trials due to formation of

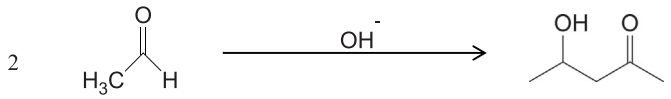

Fig. 8. Schematic representation of aldol condensation reaction.

Table 2
Color measurements of CDMOFs before and after exposure to acetaldehyde.

	L^*	a^*	b^*	ΔE
CDMOF-a	80.8 ± 2.1^a	-0.05 ± 0.1^a	-0.2 ± 0.1^a	80.8 ± 2.1^a
CDMOF-b	72.4 ± 2.6^b	-0.5 ± 0.1^a	-0.3 ± 0.3^a	72.4 ± 2.6^b
CDMOF-a encapsulated	46.9 ± 0.6^c	15.9 ± 0.4^b	39.4 ± 0.6^b	63.3 ± 0.4^c
CDMOF-b encapsulated	48.2 ± 0.8^c	-1.4 ± 0.0^c	0.9 ± 0.2^c	48.2 ± 0.8^d

Values in the same column with the same superscript letters are not significantly different at $\alpha = 0.05$.

resinous material. Researchers [36] have reported that aldehydes can undergo self-condensation reaction producing reddish-brown colored resinous material. In the case of CDMOF-b no chemical reaction has occurred. However, carboxylate moieties present in the benzoate anions bonded with hydroxyl groups present in the CDMOF-b due to hydrogen bonding as shown in Fig. 2.

3.7. Color measurements

Encapsulated CDMOF-a and CDMOF-b and activated CDMOF-a and CDMOF-b crystals were examined using the colorimeter to capture and record the color changes due to aldol condensation reaction that occurred during encapsulation of acetaldehyde in CDMOF-a. Color parameters of CDMOF-a and CDMOF-b exposed to acetaldehyde are represented in Table 2. The distinguishing color change was recorded in the encapsulated CDMOF-a, where the value of b^* yellowness and redness were very high compared to the negative values of the encapsulated CDMOF-b toward the blue and green regions, respectively. In general, the brightness values of the crystal decreased in the encapsulated samples, which is an indication of the luminosity decreasing. The redness and yellowness in the reacted CDMOF-a again supports the formation of reddish-brown colored resinous material due to the aldol condensation reaction of acetaldehyde. Color changes and acetaldehyde release from CDMOF-b did not support any chemical reaction, throughout the inclusion time and release. Thus, CDMOF-b may be suitable to build inclusion complexes for various organic compounds.

4. Conclusions

In this study, two different types of stable, accessible, high surface area and microporous sugar moiety based MOF structures with high density of reactive and accessible hydroxyl groups were synthesized. These MOF structures, CDMOF-a and CDMOF-b, were evaluated for the encapsulation of acetaldehyde and its release kinetics using GC and TGA. It was observed that CDMOF-b can successfully host and release acetaldehyde molecules into its pores. However, aldol condensation reaction was observed during encapsulation of acetaldehyde in CDMOF-a molecules, which induced color changes in CDMOF-a crystals from colorless to red color powder due to the formation of resinous material.

Acknowledgments

The authors thank Omar Dib for his insight and help during this work; Aaron Walworth, Michigan State University, for his help in

the SoP Laboratory; Edgar Castro Aguirre for his assistance with diffraction studies; and Hayati Samsudin for helping with the comments and suggestions for this work. RA thanks partial support of the USDA National Institute of Food and Agriculture and Michigan AgBioResearch, Hatch project R. Auras.

References

[1] J. Szejtli, Chem. Rev. 98 (5) (1998) 1743–1754.
[2] E.M. Del Valle, Process Biochem. 39 (2004) 1033–1046.
[3] Q.D. Hu, G.P. Tang, P.K. Chu, Acc. Chem. Res. 47 (2014) 2017–2025.
[4] B.S. Muñoz, M.A. Martìn, B. del Castillo, J.C. Menéndez, L. Vázquez, D.A. Lerner, J. Pharm. Biomed. Anal. 14 (1996) 909–915.
[5] E. Almenar, R. Auras, B. Harte, M. Rubino, US Patent No. US20070207981 A1, 2007.
[6] M.J. Joo, C. Merkel, R. Auras, E. Almenar, Int. J. Food Microbiol. 153 (2012) 297–305.
[7] M. Singh, R. Sharma, U. Banerjee, Biotechnol. Adv. 20 (2002) 341–359.
[8] F. Veiga, J. Teixeira-Dias, F. Kedzierewicz, A. Sousa, P. Maincent, Int. J. Pharm. 129 (1996) 63–71.
[9] E. Almenar, R. Auras, P. Wharton, M. Rubino, B. Harte, J. Agric. Food Chem. 55 (2007) 7205–7212.
[10] E. Almenar, R. Auras, M. Rubino, B. Harte, Int. J. Food Microbiol. 118 (2007) 164–172.
[11] S.L. James, Chem. Soc. Rev. 32 (2003) 276–288.
[12] H.K. Chae, D.Y. Siberio-Pérez, J. Kim, Y. Go, M. Eddaoudi, A.J. Matzger, M. O'Keeffe, O.M. Yaghi, Nature 427 (2004) 523–527.
[13] S.S.Y. Chui, S.M.F. Lo, J.P. Charmant, A.G. Orpen, I.D. Williams, Science 283 (1999) 1148–1150.
[14] H. Li, M. Eddaoudi, T.L. Groy, O. Yaghi, J. Am. Chem. Soc. 120 (1998) 8571–8572.
[15] H. Li, M. Eddaoudi, M. O'Keeffe, O.M. Yaghi, Nature 402 (6759) (1999) 276–279.
[16] K. Chue, J. Kim, Y. Yoo, S. Cho, R. Yang, Ind. Eng. Chem. Res. 34 (1995) 591–598.
[17] J. Moellmer, A. Moeller, F. Dreisbach, R. Glaeser, R. Staudt, Microporous Mesoporous Mater. 138 (2011) 140–148.
[18] N.L. Rosi, M. Eddaoudi, J. Kim, M. O'Keeffe, O.M. Yaghi, CrystEngComm 4 (2002) 401–404.
[19] J.F. Stoddart, R.S. Forgan, R.A. Smaldone, J.J. Gassensmith, US Patent No. 2012007904 A1, 2011.
[20] J.J. Gassensmith, H. Furukawa, R.A. Smaldone, R.S. Forgan, Y.Y. Botros, O. M. Yaghi, J.F. Stoddart, J. Am. Chem. Soc. 133 (2011) 15312–15315.
[21] S.M. Yoon, S.C. Warren, B.A. Grzybowski, Angew. Chem. Int. Ed. 53 (2014) 4437–4441.
[22] M.C. Bernini, D. Fairen-Jimenez, M. Pasinetti, A.J. Ramirez-Pastor, R.Q. Snurr, J. Mater. Chem. B 2 (2014) 766–774.
[23] C.J. Pedersen, J. Am. Chem. Soc. 89 (1967) 7017–7036.
[24] T. Ogoshi, S. Kanai, S. Fujinami, T. Yamagishi, Y. Nakamoto, J. Am. Chem. Soc. 130 (2008) 5022–5023.
[25] K. Kim, Chem. Soc. Rev. 31 (2002) 96–107.
[26] R.A. Smaldone, R.S. Forgan, H. Furukawa, J.J. Gassensmith, A.M. Slawin, O. M. Yaghi, J.F. Stoddart, Angew. Chem. Int. Ed. 49 (2010) 8630–8634.
[27] J.J. Gassensmith, J.Y. Kim, J.M. Holcroft, O.K. Farha, J.F. Stoddart, J.T. Hupp, N. C. Jeong, J. Am. Chem. Soc. 136 (2014) 8277–8282.
[28] W. Michida, M. Ezaki, M. Sakuragi, G. Guoqing, K. Kusakabe, Cryst. Res. Technol. 50 (2015) 556–559.
[29] S. Lowell, J.E. Shields, M.A. Thomas, M. Thommes, In Characterization of Porous Solids and Powders: Surface Area, Pore Size and Density, Springer (originally by Kluwer Academic Publishers), New York, 2004.
[30] E. Biemmi, S. Christian, N. Stock, T. Bein, Microporous Mesoporous Mater. 117 (2009) 111–117.
[31] N. Stock, S. Biswas, Chem. Rev. 112 (2012) 933–969.
[32] R.S. Forgan, R.A. Smaldone, J.J. Gassensmith, H. Furukawa, D.B. Cordes, Q. Li, C. E. Wilmer, Y.Y. Botros, R.Q. Snurr, A.M.Z. Slawin, J.F. Stoddart, J. Am. Chem. Soc. 134 (2012) 406–417.
[33] P. Falcaro, A.J. Hill, K.M. Nairn, J. Jasieniak, J.I. Mardel, T.J. Bastow, S.C. Mayo, M. Gimona, D. Gomez, H.J. Whitfield, R. Ricco, A. Patelli, B. Marmiroli, H. Amenitsch, T. Colson, L. Villanova, D. Buso, Nat. Commun. 2 (2010) 237.
[34] M.K. Smith, S.R. Angle, B.H. Northrop, J. Chem. Educ. 92 (2015) 368–372.
[35] Y. Wu, D. Liu, Y. Wu, H. Xi, Chem. Ind. Eng. Soc. China J. 64 (2013) 2891–2897.
[36] S.A. Ballard, V.E. Haury, Hydrogenated Ketone Resins, US Patent No. 2380142, 1945.